Radio-frequency spectroscopy of a strongly interacting spin-orbit-coupled Fermi gas

Zhengkun Fu,[1] Lianghui Huang,[1] Zengming Meng,[1] Pengjun Wang,[1] Xia-Ji Liu,[2] Han Pu,[3,4] Hui Hu,[2] and Jing Zhang[1,*]

[1]*State Key Laboratory of Quantum Optics and Quantum Optics Devices, Institute of Opto-Electronics, Shanxi University, Taiyuan 030006, People's Republic of China*

[2]*Centre for Atom Optics and Ultrafast Spectroscopy, Swinburne University of Technology, Melbourne 3122, Australia*

[3]*Department of Physics and Astronomy, and Rice Quantum Institute, Rice University, Houston, Texas 77251, USA*

[4]*Center for Cold Atom Physics, Chinese Academy of Sciences, Wuhan 430071, China*

(Received 8 September 2012; revised manuscript received 7 April 2013; published 28 May 2013)

We investigate experimentally and theoretically radio-frequency spectroscopy and pairing of a spin-orbit-coupled Fermi gas of ^{40}K atoms near a Feshbach resonance at $B_0 = 202.2$ G. Experimentally, the integrated spectroscopy is measured, showing characteristic blue and red shifts in the atomic and molecular responses, respectively, with increasing spin-orbit coupling. Theoretically, a smooth transition from atomic to molecular responses in the momentum-resolved spectroscopy is predicted, with a clear signature of anisotropic pairing at and below resonance. Our many-body prediction agrees qualitatively well with the observed spectroscopy near the Feshbach resonance.

DOI: 10.1103/PhysRevA.87.053619 PACS number(s): 67.85.−d, 03.75.Hh, 03.75.Ss, 05.30.Fk

I. INTRODUCTION

Owing to the unprecedented controllability of interaction and dimensionality, strongly interacting ultracold Fermi gases have proven to be an ideal desktop system in the study of pairing and superfluidity [1,2]. Using magnetic field Feshbach resonances, a crossover from Bose-Einstein condensates (BECs) to Bardeen-Cooper-Schrieffer (BCS) superfluids was successfully demonstrated in 2004 [3,4] and the pairing properties at the crossover have been characterized in a number of means since then, including particularly radio-frequency (rf) spectroscopy [5–7]. The latest development in this field is the realization of a synthetic spin-orbit coupling, which couples the pseudospin of neutral atoms to their orbital motion [8–12]. Such a spin-orbit coupling is responsible for a variety of intriguing phenomena in different fields of physics. A well-known example is the recently discovered topological insulators in solid state [13,14]. In the context of ultracold atomic Fermi gases, it is therefore natural to ask: What is the consequence of the interplay of strong interaction and spin-orbit coupling?

In this paper, we investigate rf spectroscopy of a strongly interacting spin-orbit-coupled Fermi gas of ^{40}K atoms. The previous works on spin-orbit-coupled Fermi gas explored essentially the noninteracting limit [11,12]. The current work is a demonstration of effects of spin-orbit coupling in an *interacting* Fermi gas. In recent BEC-BCS experiments, rf spectroscopy has been particularly useful in studying pairing and superfluidity, yielding information about the pairing gap [5] and pair size [6]. Furthermore, momentum-resolved rf spectroscopy gives direct information of the low-energy excitation spectrum and quasiparticles [7]. Here, by developing a many-body T-matrix theory we show theoretically that both atomic and molecular responses in the rf spectroscopy, arising, respectively, from free fermionic atoms and bosonic molecules, are greatly modified by spin-orbit coupling. In particular, the resulting anisotropic pairing, dominated by the two-body effect on the BEC side of the Feshbach resonance and by the many-body effect near resonance, is clearly evident in the momentum-resolved spectroscopy. Experimentally, we measure the integrated rf spectroscopy and report characteristic blue and red shifts in the atomic and molecular responses, respectively, which are in good agreement with theory.

The remainder of this paper is organized as follows. In Sec. II, we describe briefly the experimental setup and the model Hamiltonian. In Sec. III, we present the experimental and theoretical results of radio-frequency spectroscopy near Feshbach resonances. We introduce briefly a many-body T-matrix theory in Sec. III A, and in Secs. III B and III C we discuss, respectively, the integrated spectroscopy of bound molecules and the momentum-resolved spectroscopy of fermionic pairs at resonance. The comparison between experiment and theory is reported in Sec. III D. Finally, we conclude in Sec. IV. Appendix is devoted to solving the many-body T-matrix theory within the pseudogap approximation.

II. EXPERIMENTAL SETUP AND MODEL HAMILTONIAN

The experimental setup has been described in our previous works [11,15–17], in which a Bose-Fermi mixture of ^{40}K and ^{87}Rb atoms is cooled using well-developed evaporative and sympathetic cooling techniques in a quadrupole-Ioffe configuration magnetic trap, and is transported into an optical trap. A degenerate Fermi gas of about $N \simeq 2 \times 10^6$ ^{40}K atoms in the $|F = 9/2, m_F = 9/2\rangle$ internal state is evaporatively cooled to temperature $T/T_F \simeq 0.3$ with bosonic ^{87}Rb atoms, where T_F is the Fermi temperature defined by $T_F = E_F/k_B = (6N)^{1/3}\hbar\bar{\omega}/k_B$ and $\bar{\omega} \simeq 2\pi \times 130$ Hz is the geometric mean trapping frequency. ^{87}Rb atoms in the mixture are then removed by a 780-nm laser pulse. Subsequently, fermionic atoms are transferred into the lowest hyperfine state $|F = 9/2, m_F = -9/2\rangle$ via a multiphoton rapid adiabatic passage induced by a radio-frequency field at lower magnetic field. To prepare a two-component ^{40}K Fermi gas in an equal mixture of $|\uparrow\rangle = |F = 9/2, m_F = -7/2\rangle$ and $|\downarrow\rangle = |F = 9/2, m_F = -9/2\rangle$ states, a homogeneous bias magnetic field, produced by the quadrupole coils (operating in the Helmholtz

*jzhang74@yahoo.com; jzhang74@sxu.edu.cn

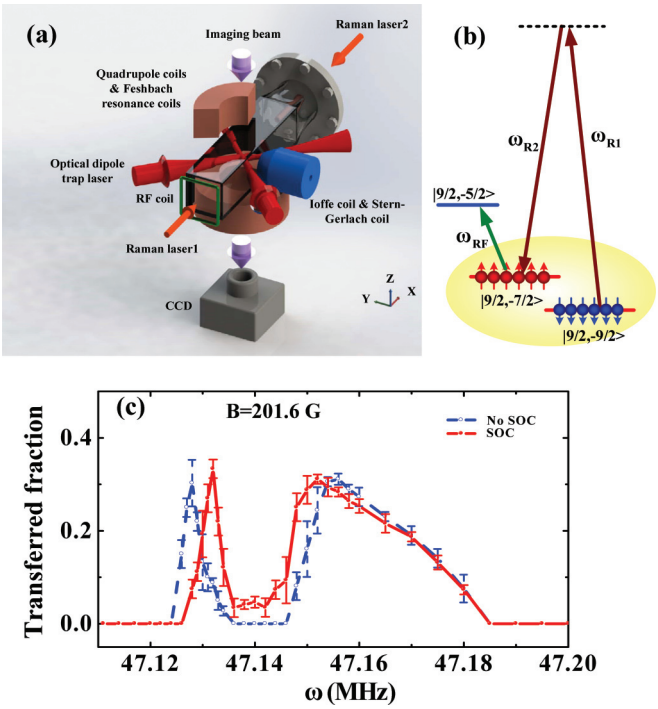

FIG. 1. (Color online) (a) and (b) Experimental realization of a strongly interacting Fermi gas of ^{40}K atoms with spin-orbit coupling. (c) The integrated rf spectroscopy below the Feshbach resonance (at $B = 201.6$ G and $a_s \simeq 2215.6a_B$, where a_B is the Bohr radius), in the presence (red solid circles) and absence (blue open circles) of the spin-orbit coupling. The Raman detuning is $\delta = 0$. The dimensionless interaction parameter $1/(k_F a_s) \simeq 0.66$. The fraction is defined as $N_{-5/2}/(N_{-5/2} + N_{-7/2})$, where $N_{-5/2}$ and $N_{-7/2}$ are obtained from the TOF absorption image. SOC, spin-orbit coupling.

configuration), is raised to about $B \approx 219.4$ G and then a radio-frequency ramp around 47.45 MHz is applied for 50 ms. To create strong interactions, the bias field is ramped from 204 G to a value near the $B_0 = 202.2$ G Feshbach resonance at a rate of about 0.08 G/ms.

We create spin-orbit coupling using the Raman process [8,11], as illustrated in Figs. 1(a) and 1(b). A pair of Raman beams from a Ti-sapphire laser counterpropagates along the $\hat{x}$ axis and couples the two spin states. The intensity of beams is $I = 50$ mW and their frequencies are shifted, respectively, by 75 and 120 MHz, using two single-pass acousto-optic modulators. These two Raman beams intersect in the atomic cloud with $1/e^2$ radii of 200 μm and are linearly polarized along $\hat{z}$ and $\hat{y}$ axis directions, respectively. The momentum transferred to atoms during the Raman process is $|\mathbf{q}_R| = 2k_R \sin(\theta/2)$, where $k_R = 2\pi/\lambda_R$ is the single-photon recoil momentum, $\lambda_R = 772.1$ nm is the wavelength, and $\theta = 180^\circ$ is the intersecting angle of two Raman beams. In the second quantization, this Raman process may be described by the term,

$$H_R = \frac{\Omega_R}{2} \int d\mathbf{r}[\psi_\uparrow^\dagger(\mathbf{r}) e^{i2k_R x} \psi_\downarrow(\mathbf{r}) + \text{H.c.}], \tag{1}$$

where $\psi_\sigma^\dagger(\mathbf{r})$ is the creation field operator for atoms in the spin-state $\sigma = \uparrow, \downarrow$ and Ω_R is the coupling strength of Raman beams. For a detailed discussion on the Raman coupling strength Ω_R, we refer to the recent theoretical work by Wei and Mueller [18].

In this paper, we use a larger bias magnetic field than the one used in our previous study [11], in order to create strong interactions. Due to a decoupling of the nuclear and electronic spins, the Raman coupling strength decreases with increasing the bias field [18]. To compensate this reduction, here we use a smaller detuning of the Raman beams with respect to the atomic "D1" transition.

To see clearly the spin-orbit coupling in our setup, it is convenient to take a gauge transformation, $\psi_\uparrow(\mathbf{r}) = e^{ik_R x}\Psi_\uparrow(\mathbf{r})$ and $\psi_\downarrow(\mathbf{r}) = e^{-ik_R x}\Psi_\downarrow(\mathbf{r})$. Our system may therefore be described by a model Hamiltonian $\mathcal{H} = \mathcal{H}_0 + \mathcal{H}_{\text{int}}$, where

$$\mathcal{H}_0 = \sum_\sigma \int d\mathbf{r}\Psi_\sigma^\dagger(\mathbf{r}) \frac{\hbar^2(\hat{\mathbf{k}} \pm k_R \mathbf{e}_x)^2}{2m} \Psi_\sigma(\mathbf{r}) + \frac{\Omega_R}{2} \int d\mathbf{r}[\Psi_\uparrow^\dagger(\mathbf{r})\Psi_\downarrow(\mathbf{r}) + \text{H.c.}] \tag{2}$$

is the single-particle Hamiltonian and

$$\mathcal{H}_{\text{int}} = U_0 \int d\mathbf{r}\Psi_\uparrow^\dagger(\mathbf{r})\Psi_\downarrow^\dagger(\mathbf{r})\Psi_\downarrow(\mathbf{r})\Psi_\uparrow(\mathbf{r}) \tag{3}$$

describes the contact interaction. In the first line of Eq. (2) we have used $\hat{\mathbf{k}} = i\nabla$, "+" for $\sigma = \uparrow$ and "−" for $\sigma = \downarrow$. Using the Pauli matrices σ_x, σ_y, and σ_z, the single-particle Hamiltonian may be rewritten in a compact form,

$$\mathcal{H}_0 = \int d\mathbf{r}\Phi^\dagger \left[\frac{\hbar^2(k_R^2 + \hat{\mathbf{k}}^2)}{2m} + h\sigma_x + \lambda k_x \sigma_z\right] \Phi, \tag{4}$$

where the spinor field operator $\Phi(\mathbf{r}) \equiv [\Psi_\uparrow(\mathbf{r}), \Psi_\downarrow(\mathbf{r})]^T$. We have defined a spin-orbit coupling constant $\lambda \equiv \hbar^2 k_R/m$ and an "effective" Zeeman field $h \equiv \Omega_R/2$.

To create a strongly interacting Fermi gas with spin-orbit coupling, after the bias magnetic field is tuned to a final value B (which is varied), we ramp up adiabatically the Raman coupling strength in 15 ms from zero to its final value $\Omega = 1.5E_R$ with Raman detuning $\delta = 0$, where the recoil energy $E_R \equiv \hbar^2 k_R^2/(2m) \simeq h \times 8.36$ kHz. The temperature of the Fermi cloud after switching on the Raman beams is at about $0.6T_F$, as in our previous measurement for a noninteracting spin-orbit-coupled Fermi gas [11]. The Fermi energy are $E_F \simeq 2.5E_R$ and the corresponding Fermi wave vector is $k_F \simeq 1.6k_R$.

III. RADIO-FREQUENCY SPECTROSCOPY

To characterize the strongly interacting spin-orbit-coupled Fermi system, we apply a Gaussian shape pulse of the rf field with a duration time about 400 μs and frequency ω to transfer the spin-up fermions to an unoccupied third hyperfine state $|3\rangle = |F = 9/2, m_F = -5/2\rangle$. The Gaussian shape pulse is generated by the voltage-controlled rf attenuators. The Gaussian envelope hence results in the elimination of the side lobes in rf spectra. The Hamiltonian for rf coupling may be written as

$$\mathcal{V}_{\text{rf}} = V_0 \int d\mathbf{r}[e^{-ik_R x}\psi_3^\dagger(\mathbf{r})\Psi_\uparrow(\mathbf{r}) + \text{H.c.}], \tag{5}$$

where $\psi_3^\dagger(\mathbf{r})$ is the field operator which creates an atom in $|3\rangle$ and V_0 is the strength of the rf drive. The effective momentum transfer $k_R\mathbf{e}_x$ in $\mathcal{V}_{\rm rf}$ results from the gauge transformation. After the rf pulse, we abruptly turn off the optical trap, the magnetic field and the Raman laser beams, and let the atoms ballistically expand for 12 ms in a magnetic field gradient applied along $\hat{z}$ and take time-of-flight (TOF) absorption image along $\hat{y}$. We measure the spin population of the final state $|3\rangle$ for different rf frequencies to obtain the rf spectra $\Gamma(\omega)$.

For a weak rf drive, the number of transferred fermions can be calculated using linear response theory. At this point, it is important to note that the final-state interactions for ^{40}K atoms in the third state and in the spin-up or spin-down state is typically small [1]. Theoretically, the rf transfer strength at a given momentum is therefore determined entirely by the single-particle spectral function of spin-up atoms $\mathcal{A}_{\uparrow\uparrow}$:

$$\Gamma(\mathbf{k},\omega) = \mathcal{A}_{\uparrow\uparrow}(\mathbf{k}+k_R\mathbf{e}_x,\epsilon_{\mathbf{k}}-\mu-\hbar\omega+\hbar\omega_{3\uparrow}) \times f(\epsilon_{\mathbf{k}}-\mu-\hbar\omega+\hbar\omega_{3\uparrow}), \quad (6)$$

where $\epsilon_{\mathbf{k}} \equiv \hbar^2k^2/(2m)$, μ is the chemical potential of the spin-orbit system, $\hbar\omega_{3\uparrow} \simeq \hbar \times 47.1$ MHz is the energy splitting between the third state and the spin-up state, $f(x) \equiv 1/(e^{x/k_BT}+1)$ is the Fermi distribution function, and we have taken the coupling strength $V_0 = 1$. For ^{6}Li atoms, however, the final state effect is usually significant [6]. The rf transfer strength will no longer be simply determined by the single-particle spectral function.

Experimentally, one could measure the momentum-resolved rf spectroscopy along the x direction $\Gamma(k_x,\omega) \equiv \sum_{k_y,k_z}\Gamma(\mathbf{k},\omega)$, or, after integration obtain the fully integrated rf spectroscopy $\Gamma(\omega) \equiv \sum_{\mathbf{k}}\Gamma(\mathbf{k},\omega)$. Due to small signal-to-noise ratio, we currently have difficulty obtaining momentum-resolved rf signal experimentally.

In Fig. 1(c), we show that the integrated rf spectroscopy of an interacting Fermi gas below the Feshbach resonance, with or without spin-orbit coupling. Here, we carefully choose the one photon detuning of the Raman lasers to avoid shifting Feshbach resonance by the Raman laser on the bound-to-bound transition between the ground Feshbach molecular state and the electronically excited molecular state. The narrow and broad peaks in the spectroscopy should be interpreted, respectively, as the rf response from free atoms and fermionic pairs. With spin-orbit coupling, we find a systematic blue shift in the atomic response and a red shift in the pair response. The latter is an unambiguous indication that the properties of fermionic pairs are strongly affected by spin-orbit coupling. In order to make sure that the observed shifts in the spectrum are induced by the spin-orbit coupling, instead of any one-photon effects, we carried out the same experiment in the presence of a pair of Raman laser beams that possess the same one-photon detuning but a much larger two-photon Raman detuning as compared to that used in Fig. 1(c). The large Raman detuning effectively destroys the spin-orbit coupling. In Fig. 2, we compare the spectrum obtained under such Raman laser beams with the one obtained without the Raman beams. The two spectra are essentially identical. This clearly demonstrates that the shifts observed in Fig. 1(c) arise from spin-orbit coupling.

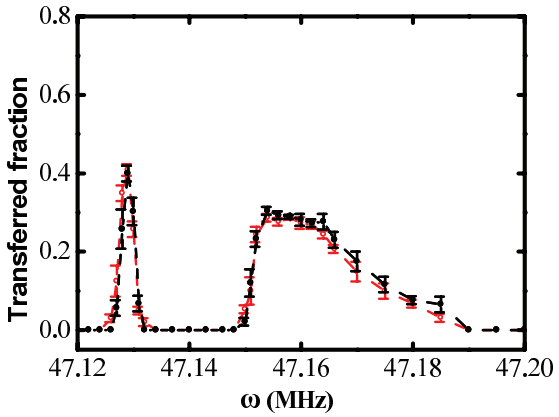

FIG. 2. (Color online) rf spectra obtained with (red open circles) and without (black solid circles) Raman laser beams with a large two-photon detuning of $\delta = 500$ kHz, but the same one-photon detuning as in Fig. 1(c).

A. Many-body T-matrix theory

Let us now consider theoretical understanding of the observed red shift for fermionic pairs. Near Feshbach resonances, it is important to treat atoms and fermionic pairs on an equal footing. For this purpose, it is convenient to develop a many-body theory within the T-matrix approximation by summing all ladder diagrams [19,20]. In the presence of spin-orbit coupling, it is necessary to define a finite-temperature Green function,

$$\mathcal{G}(\mathbf{r},\mathbf{r}';\tau>0) \equiv -\langle\Phi(\mathbf{r},\tau)\Phi^\dagger(\mathbf{r}',0)\rangle, \quad (7)$$

which is a 2 by 2 matrix even in the normal state. We adopt a partially self-consistent T-matrix scheme and take one noninteracting and one fully dressed Green function in the ladder diagrams [20]. The summation of all ladder diagrams leads to the Dyson equation,

$$\mathcal{G}(K) = \left[\mathcal{G}_0^{-1}(K) - \Sigma(K)\right]^{-1}, \quad (8)$$

where the self-energy is given by

$$\Sigma(K) = \sum_Q [t(Q)(i\sigma_y)\tilde{\mathcal{G}}_0(K-Q)(i\sigma_y)]. \quad (9)$$

Here

$$t(Q) \equiv \frac{U_0}{1+U_0\chi(Q)} \quad (10)$$

is the (scalar) T matrix with a two-particle propagator,

$$\chi(Q) = \frac{1}{2}\sum_K \mathrm{Tr}[\mathcal{G}(K)(i\sigma_y)\tilde{\mathcal{G}}_0(K-Q)(i\sigma_y)], \quad (11)$$

and the noninteracting Green function,

$$\mathcal{G}_0(K) = [i\omega_m - \epsilon_{\mathbf{k}} + \mu - E_R - h\sigma_x - \lambda k_x\sigma_z]^{-1}. \quad (12)$$

For convenience, we have used the short notations $K \equiv (\mathbf{k}, i\omega_m)$, $Q \equiv (\mathbf{q}, i\nu_n)$, and $\sum_K \equiv k_BT\sum_{\mathbf{k},\omega_m}$, and ω_m and ν_n are, respectively, the fermionic and bosonic Matsubara frequencies. We have also defined a Green function for holes, $\tilde{\mathcal{G}}(K) \equiv -[\mathcal{G}(-K)]^T$.

Equations (8)–(12) generalize the earlier T-matrix diagrammatic theory without spin-orbit coupling [20]. Here the modification arising from the spin-orbit coupling includes the use of Green functions in a general 2 by 2 matrix form and accordingly the appearance of the vertex $i\sigma_y$ in Eqs. (9) and (11). The derivation of these T-matrix equations is too technical and is not the focus of this work. Therefore, we will discuss the details of the derivation elsewhere.

In general, the self-consistent T-matrix equations are numerically difficult to solve. At a *qualitative* level, however, we may adopt a pseudogap decomposition for the T matrix [21] and obtain a set of coupled equations for the chemical potential and pairing gap. In Appendix, we discuss in detail the pseudogap approximation. By solving the coupled equations [see, i.e., Eqs. (A8) and (A9)], we calculate the single-particle spectral function,

$$\mathcal{A}_{\uparrow\uparrow}(\mathbf{k},\omega) \equiv -\frac{1}{\pi}\,\mathrm{Im}\,\mathcal{G}_{\uparrow\uparrow}(K), \tag{13}$$

and the rf-transition strengths $\Gamma(k_x,\omega)$ and $\Gamma(\omega)$. To take into account the experimental energy resolution of the spectroscopy $\gamma \sim 0.1E_R$ [12], we replace the Dirac delta function [which appears in $\mathcal{A}_{\uparrow\uparrow}(\mathbf{k},\omega)$] by

$$\delta(x) = \frac{\gamma/\pi}{x^2+\gamma^2}. \tag{14}$$

B. Integrated spectroscopy of bound molecules

In Fig. 3, we predict the integrated rf spectroscopy of a spin-orbit-coupled Fermi gas at $B = 201.6$ G and $T = 0.6T_F$. With increasing the strength of Raman beams from 0 to $4E_R$, the atomic and pair peaks shift to the higher and lower frequencies, respectively, in qualitative agreement with the experimental observation in Fig. 1(c). At this interaction parameter $[1/(k_F a_s) \simeq 0.66]$, the red shift of pair peaks may be understood from the binding energy of pairs in the two-body limit: the stronger effective Zeeman field h, the smaller binding energy of two-particle bound states [22]. In the inset, we show the prediction of the momentum-resolved rf spectroscopy at $\Omega_R = 2E_R$. It is highly asymmetric as a function of momentum. The predicted atomic response is in good agreement with the experimental observation for a noninteracting spin-orbit-coupled Fermi gas [11,12].

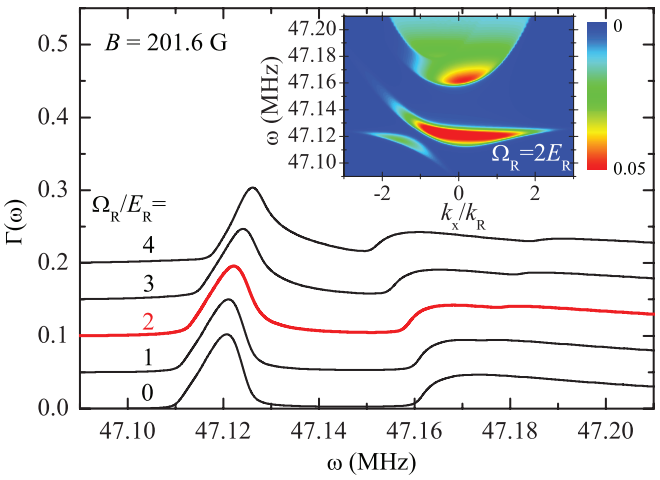

FIG. 3. (Color online) Evolution of the predicted integrated rf spectroscopy as a function of the Raman coupling strength. Here, $1/k_F a_s = 0.66$, $T = 0.6T_F$, and $k_F = 1.6k_R$. The inset shows a linear contour plot of the predicted momentum-resolved spectroscopy at $\Omega_R = 2E_R$.

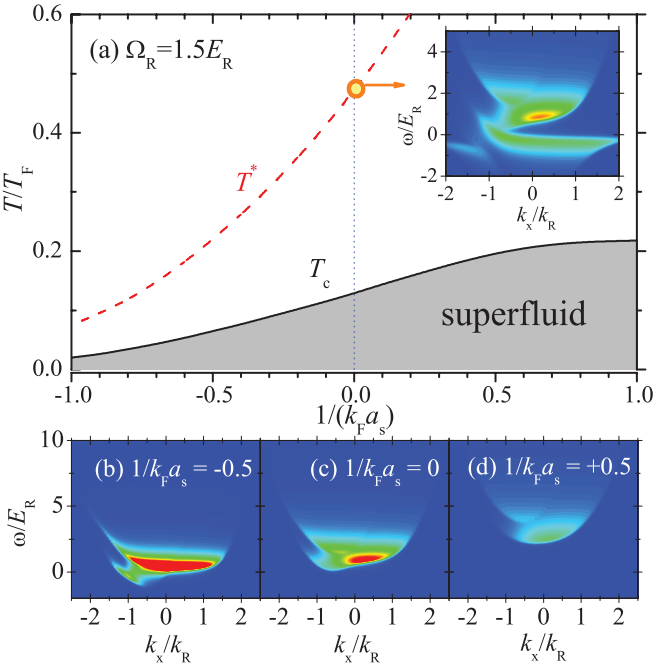

FIG. 4. (Color online) (a) Predicted phase diagram of a strongly interacting spin-orbit-coupled Fermi gas at $\Omega_R = 1.5E_R$ and $k_F = 1.6k_R$. (b)–(d) Linear contour plots of the zero temperature momentum-resolved rf spectroscopy across the Feshbach resonance, in arbitrary units. The inset in (a) shows the momentum-resolved rf spectroscopy at the pseudgap temperature T^* in the unitary limit. In theoretical calculations, we have set $\omega_{3\uparrow} = 0$.

C. Momentum-resolved spectroscopy near Feshbach resonances

We now turn to the rf spectroscopy in the vicinity of the Feshbach resonance. In Fig. 4(a), we plot the superfluid transition temperature T_c and the pairing breaking (pseudogap) temperature T^* of a spin-orbit-coupled Fermi gas at $\Omega_R = 1.5E_R$ and $k_F = 1.6k_R$. The pseudogap temperature is calculated using the standard BCS mean-field theory without taking into account the preformed pairs (i.e., $\Delta_{pg} = 0$) [21]. We find that the region of superfluid phase is suppressed by spin-orbit coupling. In particular, at resonance the superfluid transition temperature is about $T_c \simeq 0.129T_F$, smaller than the measured value of $T_c \simeq 0.167(13)T_F$ [23] or the predicted value of $T_c \simeq 0.15T_F$ (under the same pseudogap approximation) for a unitary Fermi gas in the absence of spin-orbit coupling. Thus, experimentally it becomes more challenge to observe a spin-orbit-coupled fermionic superfluid in the present experimental scheme.

In Figs. 4(b)–4(d), we show the zero-temperature momentum-resolved rf-spectroscopy across the resonance. On the BCS side $(1/k_F a_s = -0.5)$, the spectroscopy is dominated by the response from atoms and shows a characteristic

high-frequency tail at $k_x < 0$ [11,12,24]. Towards the BEC limit ($1/k_F a_s = 0.5$), the spectroscopy may be understood from the picture of well-defined pairs and shows a clear twofold anisotropic distribution [25]. The spectroscopy at the resonance is complicated and should be attributed to many-body fermionic pairs. The change of spectroscopy across resonance is continuous, in accord with a smooth BEC-BCS crossover [2].

In the inset of Fig. 4(a), we show the momentum-resolved rf spectroscopy at the resonance and at the pseudogap pairing temperature T^*. It is interesting that the anisotropic distribution survives well above the superfluid transition temperature T_c. An experimental observation of such a spectroscopy would be a strong indication of the anisotropic *pseudogap* pairing of a spin-orbit-coupled Fermi gas in its normal state.

D. Experiment vs theory

In Fig. 5, we examine our many-body theory by comparing the theoretical predictions with the experimental data for integrated rf spectroscopy. At the qualitative level, we do not consider the trap effect and take the relevant experimental parameters at the trap center. Otherwise, there are no adjustable free parameters used in the theoretical calculations. As shown in Fig. 5, we find a qualitative agreement between theory and

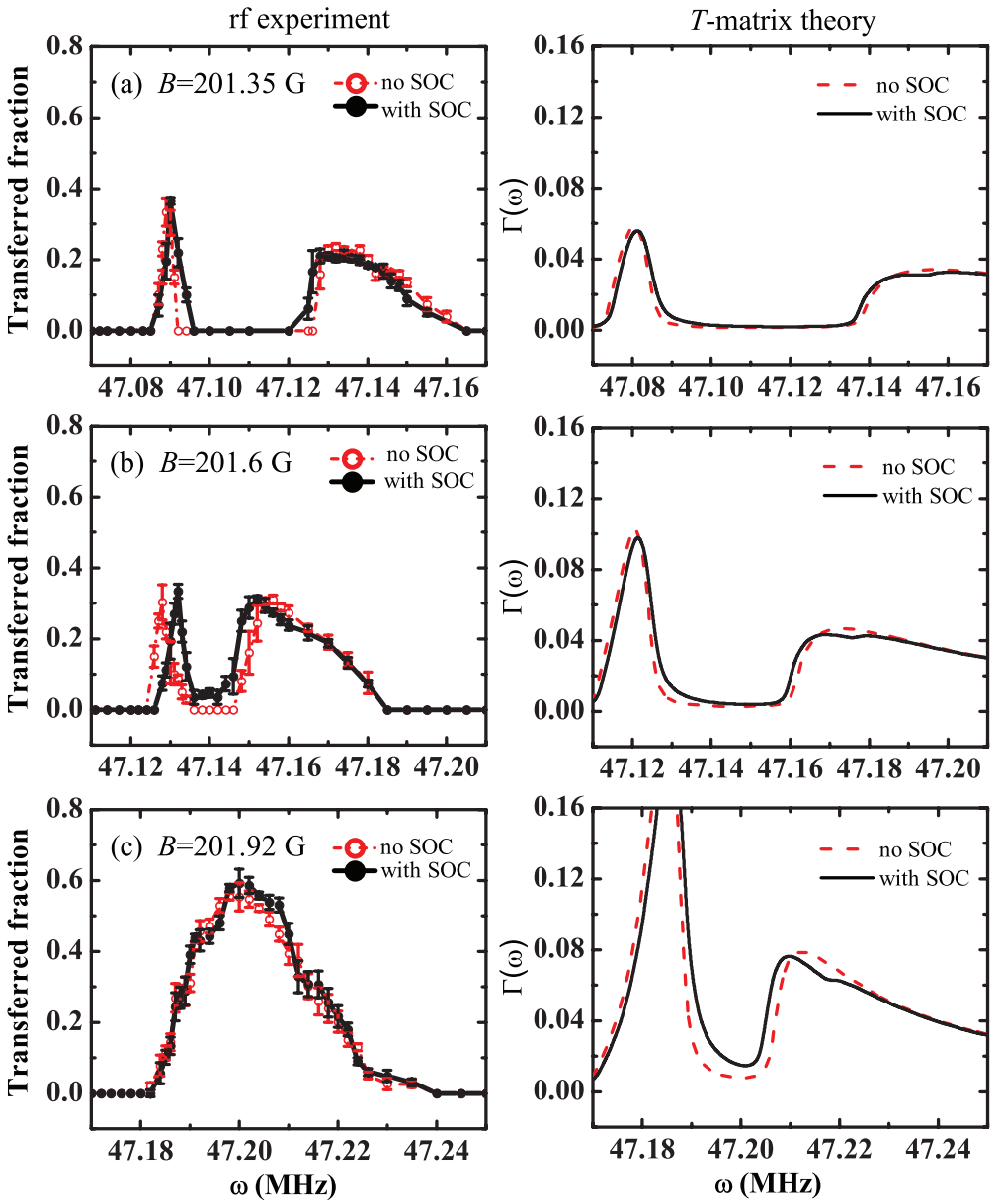

FIG. 5. (Color online) Comparison between theory and experiment for the integrated rf spectroscopy. In theoretical simulations, we use $\Omega_R = 1.5E_R$, $k_F = 1.6k_R$, and $T = 0.6T_F$, according to the experimental setup. The red solid circles (red solid lines) and dark open circles (dark dashed lines) show, respectively, the experimental data (theoretical predictions) in the presence and absence of spin-orbit coupling with Raman detuning $\delta = 0$. The dimensionless interaction parameter $1/(k_F a_s)$ in (a), (b), and (c) are 0.89, 0.66, and 0.32, respectively.

experiment, both of which show the red shift of the response from fermionic pairs. As we have already discussed in Sec. III B, a red shift of the pairing response may be understood from the two-body limit. Its prediction or existence therefore seems to depend weakly on the accuracy of the theory. Note that, near Feshbach resonances our many-body pseudogap theory is only qualitatively reliable. It cannot explain well the separation of atomic and pair peaks in the observed integrated rf spectrum. More seriously, it fails to take into account properly the strong interactions between atoms and pairs [see, for example, Fig. 5(c)]. However, our theory does reproduce exactly the two-body result in the BEC limit and thus capture the essential feature of the red shift due to spin-orbit coupling.

IV. CONCLUSION

In conclusion, we have investigated experimentally and theoretically rf spectroscopy and fermionic pairing in a strongly interacting spin-orbit-coupled Fermi gas of ^{40}K atoms near a Feshbach resonance. A red shift of the response from fermionic pairs, induced by spin-orbit coupling, is observed in integrated rf spectroscopy below the resonance, in qualitative agreement with a many-body T-matrix calculation. Momentum-resolved rf spectroscopy of fermionic pairs has been predicted across the resonance at all temperatures, showing a characteristic anisotropic distribution. This is to be confronted in future experiments.

We note that the typical experimental temperature in this work is about $0.6T_F$. In the future, we wish to reduce the temperature of the strongly interacting Fermi cloud of ^{40}K atoms down to $0.2T_F$, close to the superfluid transition. This is encouraged by a recent calculation by Wei and Mueller [18], who showed that the heating of the cloud due to Raman transition is not significantly affected by the magnetic field needed for Feshbach resonances.

Theoretically, it is possible to solve the many-body T-matrix theory without the pseudogap approximation. On the other hand, at the relatively high temperature $T \sim 0.6T_F$, alternatively we may use a virial expansion theory to obtain quantitative predictions for the radio-frequency spectroscopy in harmonic traps [27–29]. These possibilities will be addressed in later studies.

ACKNOWLEDGMENTS

We thank Zeng-Qiang Yu and Hui Zhai for useful discussions. This research is supported by National Basic Research Program–China (Grant No. 2011CB921601), National Natural Science Foundation of China (NSFC) Project for Excellent Research Team (Grant No. 61121064), NSFC (Grant No. 11234008), Doctoral Program Foundation of Ministry of Education China (Grant No. 20111401130001). X.J.L. and H.H. are supported by the Australian Research Council (ARC) Discovery Projects (Grants No. DP0984637 and No. DP0984522). H.P. is supported by the National Science Foundation and the Welch Foundation (Grant No. C-1669).

APPENDIX: PSEUDOGAP APPROXIMATION

The pseudogap approximation is advanced by the Chicago group [21]. In this approximation the T matrix is separated into two parts, $t(Q) = t_{sc}(Q) + t_{pg}(Q)$, so that the contribution from the superfluid order parameter for condensed pairs Δ_{sc}^2,

$$t_{sc}(Q) = -\frac{\Delta_{sc}^2}{T}\delta(Q), \tag{A1}$$

and the contribution from the pseudogap for uncondensed pairs,

$$\Delta_{pg}^2 \equiv -\sum_{Q\neq 0} t_{pg}(Q), \tag{A2}$$

become explicit. The full pairing order parameter is given by $\Delta^2 = \Delta_{sc}^2 + \Delta_{pg}^2$. Accordingly, we have the self-energy $\Sigma(K) = \Sigma_{sc}(K) + \Sigma_{pg}(K)$ [21], where

$$\Sigma_{sc} = -\Delta_{sc}^2(i\sigma_y)\tilde{\mathcal{G}}_0(K)(i\sigma_y) \tag{A3}$$

and

$$\Sigma_{pg} = -\Delta_{pg}^2(i\sigma_y)\tilde{\mathcal{G}}_0(K)(i\sigma_y). \tag{A4}$$

To obtain Σ_{pg} in the above equation, it is assumed that the pair propagator $\chi(Q)$ peaks around $Q = 0$ [21].

We note that, at zero temperature the pseudogap approximation is simply the standard mean-field BCS theory, in which

$$\Sigma(K) = -\Delta^2(i\sigma_y)\tilde{\mathcal{G}}_0(K)(i\sigma_y). \tag{A5}$$

Above the superfluid transition, however, it captures the essential physics of fermionic pairing and therefore should be regarded as an improved theory beyond mean field.

To calculate the pseudogap Δ_{pg}, we approximate

$$t_{pg}^{-1}(Q \simeq 0) = \mathcal{Z}[i\nu_n - \Omega_{\mathbf{q}} + \mu_{\text{pair}}], \tag{A6}$$

where the residue $\mathcal{Z}$ and the effective dispersion of pairs $\Omega_{\mathbf{q}} = \hbar^2 q^2/2M^*$ are to be determined by expanding $\chi(Q)$ about $Q = 0$ [21,26]. The form of $t_{pg}(Q)$ leads to

$$\Delta_{pg}^2(T) = \mathcal{Z}^{-1}\sum_{\mathbf{q}} f_B(\Omega_{\mathbf{q}} - \mu_{\text{pair}}), \tag{A7}$$

where $f_B(x) \equiv 1/(e^{x/k_BT} - 1)$ is the bosonic distribution function. We arrive finally at two coupled equations, the gap equation,

$$\frac{1}{U_0} + \chi(Q = 0) = \mathcal{Z}\mu_{\text{pair}}, \tag{A8}$$

and the number equation,

$$n = \sum_K \text{Tr}\mathcal{G}(K), \tag{A9}$$

to determine the superfluid order parameter Δ_{sc} and the chemical potential μ, respectively, for a given set of parameters.

[1] I. Bloch, J. Dalibard, and W. Zwerger, Rev. Mod. Phys. **80**, 885 (2008).
[2] S. Giorgini, L. P. Pitaevskii, and S. Stringari, Rev. Mod. Phys. **80**, 1215 (2008).
[3] C. A. Regal, M. Greiner, and D. S. Jin, Phys. Rev. Lett. **92**, 040403 (2004).
[4] M. W. Zwierlein, C. A. Stan, C. H. Schunck, S. M. F. Raupach, A. J. Kerman, and W. Ketterle, Phys. Rev. Lett. **92**, 120403 (2004).
[5] C. Chin, M. Bartenstein, A. Altmeyer, S. Riedl, S. Jochim, J. Hecker Denschlag, and R. Grimm, Science **305**, 1128 (2004).
[6] C. H. Schunck, Y. Shin, A. Schirotzek, and W. Ketterle, Nature (London) **454**, 739 (2008).
[7] J. T. Stewart, J. P. Gaebler, and D. S. Jin, Nature (London) **454**, 744 (2008).
[8] Y.-J. Lin, K. Jiménez-García, and I. B. Spielman, Nature (London) **471**, 83 (2011).
[9] Z. Fu, P. Wang, S. Chai, L. Huang, and J. Zhang, Phys. Rev. A **84**, 043609 (2011).
[10] J. Y. Zhang, S. C. Ji, Z. Chen, L. Zhang, Z. D. Du, B. Yan, G. S. Pan, B. Zhao, Y. J. Deng, H. Zhai, S. Chen, and J. W. Pan, Phys. Rev. Lett. **109**, 115301 (2012).
[11] P. Wang, Z.-Q. Yu, Z. Fu, J. Miao, L. Huang, S. Chai, H. Zhai, and J. Zhang, Phys. Rev. Lett. **109**, 095301 (2012).
[12] L. W. Cheuk, A. T. Sommer, Z. Hadzibabic, T. Yefsah, W. S. Bakr, and M. W. Zwierlein, Phys. Rev. Lett. **109**, 095302 (2012).
[13] X.-L. Qi and S.-C. Zhang, Phys. Today **63**, 33 (2010).
[14] M. Z. Hasan and C. L. Kane, Rev. Mod. Phys. **82**, 3045 (2010).
[15] D. Xiong, H. Chen, P. Wang, X. Yu, F. Gao, and J. Zhang, Chin. Phys. Lett. **25**, 843 (2008).
[16] D. Xiong, P. Wang, Z. Fu, S. Chai, and J. Zhang, Chin. Opt. Lett. **8**, 627 (2010).
[17] P. Wang, L. Deng, E. W. Hagley, Z. Fu, S. Chai, and J. Zhang, Phys. Rev. Lett. **106**, 210401 (2011).
[18] R. Wei and E. J. Mueller, Phys. Rev. A **87**, 042514 (2013).
[19] H. Hu, X.-J. Liu, and P. D. Drummond, Phys. Rev. A **77**, 061605(R) (2008).
[20] H. Hu, X.-J. Liu, and P. D. Drummond, New J. Phys. **12**, 063038 (2010).
[21] Q. J. Chen, J. Stajic, S. Tan, and K. Levin, Phys. Rep. **412**, 1 (2005).
[22] L. Jiang, X.-J. Liu, H. Hu, and H. Pu, Phys. Rev. A **84**, 063618 (2011).
[23] M. J. H. Ku, A. T. Sommer, L. W. Cheuk, and M. W. Zwierlein, Science **335**, 563 (2012).
[24] X.-J. Liu, Phys. Rev. A **86**, 033613 (2012).
[25] H. Hu, H. Pu, J. Zhang, S.-G. Peng, and X.-J. Liu, Phys. Rev. A **86**, 053627 (2012).
[26] At the qualitative level, we approximate the effective mass of pairs, $M^* = 2m$.
[27] X.-J. Liu, H. Hu, and P. D. Drummond, Phys. Rev. Lett. **102**, 160401 (2009).
[28] H. Hu, X.-J. Liu, P. D. Drummond, and H. Dong, Phys. Rev. Lett. **104**, 240407 (2010).
[29] X.-J. Liu, Phys. Rep. **524**, 37 (2013).